Aerodynamic Shape Optimization of a Flying-Wing UAV

*AN Yingtao, MU Xusheng, ZHAO Yonghui**

College of Aerospace Engineering, Nanjing University of Aeronautics and Astronautics, Nanjing 210016, P. R. China

(Received 10 May 2023; revised 30 August 2023; accepted 7 October 2023)

Abstract: The flying-wing layout, characterized by its distinctive aerodynamic fusion of the wing and fuselage, markedly augments the effective lift surface area of an aircraft. Both shape optimization and layout optimization play equally vital roles in enhancing the aerodynamic performance of this kind of configurations. In this paper, to address the aerodynamic shape optimization challenges pertaining to flying-wing unmanned aerial vehicle (UAV), an efficient parametric modeling method is introduced. This method facilitates the parametric deformation control of complex shapes. It integrates gradient-based optimization algorithms, discrete adjoint methods, and computational fluid dynamics (CFD) techniques grounded in Reynolds average Navier-Stokes (RANS) equations to achieve aerodynamic shape optimization and reduce drag for flying-wing UAV, resulting in a notable 7.17% improvement in the lift-to-drag ratio. The optimization results indicate that, while adhering to constraint requirements, the aerodynamic optimization design method based on these methodologies exhibits robust adaptability to wing-fuselage blended configurations, effectively enhancing the aerodynamic performance of unmanned aerial vehicles.

Key words: flying-wing layout; aerodynamic optimization; computational fluid dynamics; discrete adjoint; free-form deformation

CLC number: V211.3 **Document code:** A **Article ID:** 1005-1120(2023)S2-0009-09

0 Introduction

With the rapid advancement of aeronautical science and technology, the demands for improved aerodynamic efficiency in aircraft performance have been steadily escalating. This escalation is evident in the heightened complexity of constraints and the increasingly stringent performance criteria imposed upon aerodynamic design, resulting in the emergence of more intricate constraints and the necessity to harmonize multiple design objectives. In the 1970s, a period marked by significant advancements in computer performance and the maturation of large-scale parallel computing technology, the computational fluid dynamics (CFD) methodology began to intersect with optimization algorithms, giving birth to the field of aerodynamic shape optimization design technology. Aerodynamic shape optimization represents the culmination of multidisciplinary integration, drawing from fields such as aerodynamics, optimization theory, computer technology, and machine learning. Its role is to translate engineering performance criteria and constraints into mathematical formulations that optimization algorithms can process, thereby providing a robust technical framework for aircraft design and diminishing the designers' reliance on experiential knowledge. In essence, aerodynamic design optimization strives to identify the optimal aerodynamic profile design that conforms to predefined constraints[1].

In 1978, Hicks and Henne[2] pioneered the field of aerodynamic shape optimization for wing designs. Subsequently, the optimization of wing shapes was pursued by Leung and Zingg, who employed the parallel Newton-Krylov method[3]. In addressing the challenge of multi-objective optimization, Nemec et al.[4] utilized the weight superposition method to conduct multi-point and multi-objective optimization for wing shapes. In the realm of

*Corresponding author, E-mail address: zyhae@nuaa.edu.cn.

How to cite this article: AN Yingtao, MU Xusheng, ZHAO Yonghui. Aerodynamic shape optimization of a flying-wing UAV [J]. Transactions of Nanjing University of Aeronautics and Astronautics, 2023, 40(S2): 9-17.

http://dx.doi.org/10.16356/j.1005-1120.2023.S2.002

handling complex geometries and employing efficient optimization techniques, Chang et al.[5] employed the free-form deformation (FFD) method and genetic algorithms to perform aerodynamic optimization for secondary folding wings of pipe-launched unmanned aerial vehicles (UAVs). This paper extends the application of the aforementioned methods to the design of a flying-wing UAV. Commencing from the geometric baseline of the flying-wing UAV, we implement a geometric parameterization of the aircraft's shape using the FFD method. The Reynolds average Navier-Stokes (RANS) equation is solved using the CFD method, and gradient information derived from the discrete adjoint method. Consequently, this study achieves efficient and high-fidelity aerodynamic shape optimization for the flying-wing UAV, laying a solid foundation for subsequent stages of the overall design process.

1 Methodology

1.1 Geometry parameterization

Geometry parameterization is a technique employed to depict the shape and its alterations by utilizing specific parameters aligned with the aerodynamic properties of the geometric model. In this particular study, the FFD method is employed to actualize the geometric parameterization of the aircraft's form[6]. The FFD method, initially introduced by Sederberg and Parry in 1986[7], constitutes a parameterization approach rooted in the concept of unrestricted deformation and enjoys widespread adoption within the realm of computer graphics.

In its essence, this approach achieves the bulk modification of surface mesh point coordinates by effecting changes in the positions of FFD control points, bypassing direct manipulation of the surface mesh. This strategic approach not only reduces the number of required control points but also minimizes discontinuities, thereby enhancing the smoothness of deformations. Sederberg and Parry utilized a rectangular framework with $l+1$, $m+1$, and $n+1$ nodes distributed along its length, width, and height dimensions, respectively, to serve as the control volume. The objects under investigation are enclosed within this control volume, and the $(l+1)\times(m+1)\times(n+1)$ nodes are designated as control points. A systematic functional relationship governs the association between the control points and the coordinates of each node within the framework. The manipulation of control point positions leads to the computation of new positions for every node within the framework based on this functional relationship.

Within the mathematical context, FFD is formally defined as the tensor product of three Bernstein polynomials. Our initial step involves the establishment of a local coordinate system on a parametric domain, any point within the local coordinate system remain constant, as can be expressed as

$$\boldsymbol{X}=\boldsymbol{X}_0+s\boldsymbol{S}+t\boldsymbol{T}+u\boldsymbol{U} \tag{1}$$

where $\boldsymbol{X}_0$ represents the global coordinates of the control point, while s, t, and u correspond to the local coordinates within the coordinate system established at the control point, and they satisfy that $0\leqslant s\leqslant 1$, $0\leqslant t\leqslant 1$, $0\leqslant u\leqslant 1$. $\boldsymbol{S}$, $\boldsymbol{T}$, and $\boldsymbol{U}$ denote the three-axis vectors of the local coordinate system, respectively.

$$\begin{cases} s=\dfrac{\boldsymbol{T}\times\boldsymbol{U}(\boldsymbol{X}-\boldsymbol{X}_0)}{\boldsymbol{T}\times\boldsymbol{U}\times\boldsymbol{S}} \\ t=\dfrac{\boldsymbol{S}\times\boldsymbol{U}(\boldsymbol{X}-\boldsymbol{X}_0)}{\boldsymbol{S}\times\boldsymbol{U}\times\boldsymbol{T}} \\ u=\dfrac{\boldsymbol{S}\times\boldsymbol{T}(\boldsymbol{X}-\boldsymbol{X}_0)}{\boldsymbol{S}\times\boldsymbol{T}\times\boldsymbol{U}} \end{cases} \tag{2}$$

Assuming an even distribution of control points along every edge, the coordinates of these control points in the global coordinate system are as follows

$$\boldsymbol{P}_{i,j,k}=\boldsymbol{X}_0+\frac{i}{l}\boldsymbol{S}+\frac{j}{m}\boldsymbol{T}+\frac{k}{n}\boldsymbol{U} \tag{3}$$

The alteration of control point coordinates permits the modification of coordinates for corresponding surface nodes on the geometric object. When adjustments are made to the positions of FFD control points to create displacement vectors $\Delta\boldsymbol{P}_{i,j,k}$, the change in displacement of any grid point with local coordinates can be accurately calculated using the following equation

$$\Delta\boldsymbol{X}(s,t,u)=\sum_{i=0}^{l}\sum_{j=0}^{m}\sum_{k=0}^{n}\Delta\boldsymbol{P}_{i,j,k}\boldsymbol{N}_i(s)\boldsymbol{N}_j(t)\boldsymbol{N}_k(u) \tag{4}$$

The coordinates of the newly positioned grid points are determined through the positions of the

updated control points, identified as $\boldsymbol{P}_{i,j,k}$, so we have

$$\boldsymbol{X}(s,t,u)=\sum_{i=0}^{l}\sum_{j=0}^{m}\sum_{k=0}^{n}\boldsymbol{P}_{i,j,k}\boldsymbol{N}_i(s)\boldsymbol{N}_j(t)\boldsymbol{N}_k(u) \quad (5)$$

Within the given equation, $\boldsymbol{N}_i(s)$, $\boldsymbol{N}_j(t)$, and $\boldsymbol{N}_k(u)$ have the potential to function as Bernstein polynomials defined on the parametric space (s, t, u). Nevertheless, the B-spline basis functions or various polynomial forms may also be considered.

Owing to the characteristics of Bernstein functions, the FFD approach boasts a high degree of deformation continuity and smoothness. Furthermore, due to the nature of overall deformation within the elastic body, when parameterizing the entire model, the FFD method not only facilitates continuous geometric shape adjustments by manipulating the control point positions but also concurrently deforms the flow field mesh alongside the geometry. Therefore, there is no need to regenerate the flow field mesh. Fig.1 illustrates the grids and the FFD control volume of the initial configuration of the flying-wing UAV examined in this study.

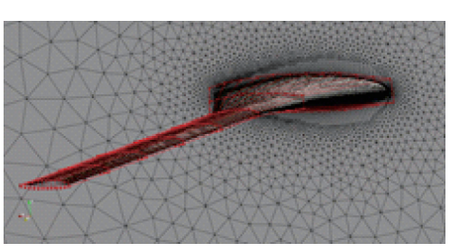

Fig.1 Flow field grids and the FFD control volume for the initial configuration of the flying-wing UAV

1.2 Flow field solution method

In this study, we employ the improved open-source RANS CFD code known as DAFoam[8-9] to address the flow field. DAFoam, serving as a second-order finite-volume solver, is capable of solving the Euler, Navier-Stokes (N-S), and RANS equations in both steady and unsteady states, while also providing adaptive wall functions. To ensure high physical fidelity, we utilize the RANS equation for our investigation. Considering the specific operating conditions of our research, we opt for the Spalart-Allmaras (S-A) one-equation model within the incompressible RANS turbulence framework. The S-A model, designed for wall-bound flows, simplifies the solution of dynamic vortex viscosity issues by incorporating a new set of equations that do not involve the calculation of the length scale associated with the shear stress layer thickness. This model, primarily intended for aviation applications, has demonstrated promising outcomes in recent studies.

1.3 Optimization algorithm

Computational expenses associated with CFD simulations are notably high, emphasizing the pivotal importance of selecting an effective optimization algorithm that minimizes the number of function calls. Non-gradient methods, such as genetic algorithms, are better suited for scenarios featuring multiple local minima. Nevertheless, they exhibit slow convergence rates and require a substantial number of function calls, rendering them impractical for cases involving a high number of design variables, as encountered in this study. In contrast, gradient-based methods are widely favored for their superior optimization efficiency. These methods leverage gradient information to determine the search direction for the objective function, thereby achieving optimization. In an optimization problem featuring m design variables and n constraints, the objective function generates $n\times m$ gradient values. Therefore, efficiently and accurately obtaining gradient information for numerous design variables is of paramount importance.

Jameson[10] originally introduced the adjoint method to aerodynamic shape optimization research. This method requires solving the flow equation and the adjoint equation only once to obtain the partial derivatives of the objective function with respect to all design variables. Furthermore, as the computational effort for gradient computation is comparable to that of the flow solution, the total computational cost of the adjoint method is approximately equal to twice the cost of flow computations. Additionally, it is independent of the dimensionality of the design variables, effectively resolving the "dimensionality disaster" and enabling the rapid optimization of com-

plex aerodynamic shapes with multiple variables[11].

Furthermore, adjoint methods can be categorized into continuous adjoint methods and discrete adjoint methods, depending on whether the governing equations are continuous or discrete. While the continuous adjoint method offers faster solution speeds, it tends to exhibit weaker solution accuracy compared to the discrete adjoint method, making it challenging to apply in complex flow scenarios like turbulence models. Consequently, this paper opts for the discrete adjoint method to address the governing equations.

In the pursuit of solving the optimization problem at hand, it becomes imperative to ascertain the derivative of the objective function concerning the design variables. This derivative, denoted as $\mathrm{d}f/\mathrm{d}\boldsymbol{x}$, necessitates considering the function f in relation to both the design variables $\boldsymbol{x}=[x_1, x_2, \cdots, x_{N_x}]^{\mathrm{T}}$ and the state variables $\boldsymbol{w}=[w_1, w_2, \cdots, w_{N_w}]^{\mathrm{T}}$. Specifically, within the domain of aerodynamic shape optimization, the design variables $\boldsymbol{x}$ represent the spatial coordinates of FFD control points. These coordinates are inherently linked to the state variables $\boldsymbol{w}$ characterizing the flow field. Typically, the objective function f pertains to aerodynamic coefficients, such as the drag coefficient C_{D}. The application of the chain rule allows us to express the derivative of the objective function with respect to the design variables $\boldsymbol{x}$ as

$$\frac{\mathrm{d}f}{\mathrm{d}\boldsymbol{x}}=\frac{\partial f}{\partial \boldsymbol{x}}+\frac{\partial f}{\partial \boldsymbol{w}}\frac{\partial \boldsymbol{w}}{\partial \boldsymbol{x}} \tag{6}$$

In the quest to calculate $\mathrm{d}f/\mathrm{d}\boldsymbol{x}$, it becomes imperative to tackle a system of N_x equations (N_x being the number of design variables). To streamline computational expenses, our strategy involves establishing the residual of the flow control equations as equal to zero. In essence, we seek to solve $R[\boldsymbol{w}, \boldsymbol{x}]=0$ and subsequently linearize this expression to acquire the derivative

$$\frac{\partial \boldsymbol{R}}{\partial \boldsymbol{w}}\frac{\partial \boldsymbol{w}}{\partial \boldsymbol{x}}=-\frac{\partial \boldsymbol{R}}{\partial \boldsymbol{x}} \tag{7}$$

where $\boldsymbol{R}$ represents the residual, and $\mathrm{d}\boldsymbol{R}/\mathrm{d}\boldsymbol{w}$ is an $N_w \times N_w$ matrix that can be obtained by solving a linear equation system to find $\partial \boldsymbol{w}/\partial \boldsymbol{x}$, here N_w is the flow field dimension. Assuming the existence of an N_x-dimensional vector $\boldsymbol{\xi}$ that satisfies

$$\left(\frac{\partial \boldsymbol{R}}{\partial \boldsymbol{w}}\right)^{\mathrm{T}}\boldsymbol{\xi}=\left(\frac{\partial f}{\partial \boldsymbol{w}}\right)^{\mathrm{T}} \tag{8}$$

It can be obtained from the above equation

$$\boldsymbol{\xi}^{\mathrm{T}}=\frac{\partial f}{\partial \boldsymbol{w}}\left(\frac{\partial \boldsymbol{R}}{\partial \boldsymbol{w}}\right)^{-1} \tag{9}$$

Further, by combining Eqs.(6) and (7), we obtain

$$\frac{\mathrm{d}f}{\mathrm{d}\boldsymbol{x}}=\frac{\partial f}{\partial \boldsymbol{x}}-\frac{\partial f}{\partial \boldsymbol{w}}\left(\frac{\partial \boldsymbol{R}}{\partial \boldsymbol{w}}\right)^{-1}\frac{\partial \boldsymbol{R}}{\partial \boldsymbol{x}} \tag{10}$$

Continuing with reference to Eq.(8), one can readily obtain the following expression

$$\frac{\mathrm{d}f}{\mathrm{d}\boldsymbol{x}}=\frac{\partial f}{\partial \boldsymbol{x}}+\boldsymbol{\xi}^{\mathrm{T}}\frac{\partial \boldsymbol{R}}{\partial \boldsymbol{x}} \tag{11}$$

As depicted in Eq.(8), the gradient of the objective function f concerning any design variable $\boldsymbol{x}$ can be derived using Eq.(11) by solving the linear equation system once to acquire the vector $\boldsymbol{\xi}$. Since Eq.(11) predominantly comprises vector multiplication operations, the computational time required for Eq.(11) is negligible. Thus, the problem that initially involved solving N_x linear equations now simply entails solving the linear equations once, specifically, the adjoint Eq.(8).

Employed within this study is the classical sequential quadratic programming method, a gradient-based optimization algorithm renowned for its attributes of computational efficiency, robust convergence, reliability, and a robust boundary search capability. This method effectively transforms the complex nonlinear constrained optimization problem into a more tractable quadratic programming task, progressively approximating the solution. The open-source multidisciplinary optimization platform, Mach-Aero[6], is harnessed in this paper to orchestrate the integration of each component of the optimization problem. Fig.2 illustrates the optimization process. The changeable parameters are represented by the blue rhombus, while the operational procedure is illustrated by the white rectangle.

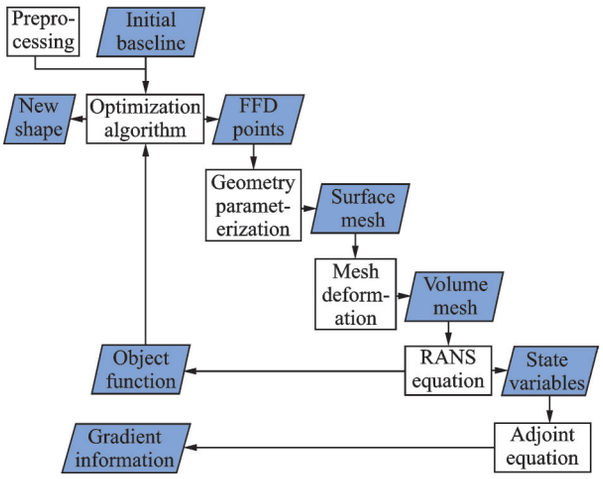

Fig.2 Workflow of aerodynamic optimization design

2 Aerodynamic Shape Optimization Problem Setting

2.1 Initial geometric shape

An initial geometric layout of the UAV, shown in Fig.1, is segmented into three components: the fuselage, inner wing, and outer wing. Its wingspan measures 4 m, with an aspect ratio of 6.8, and a sweep angle of 22°.

2.2 Flow field solution

Due to the susceptibility of the flying-wing UAV under study to experience flutter phenomena at very low flight speeds, it can only maintain a cruise state at relatively low Mach numbers. Cruise conditions are selected with a Mach number $Ma = 0.1$, an angle of attack $\alpha = 1°$, and a Reynolds number $Re = 1\ 055\ 830$. The choice of discrete schemes is as follows: for time discretization, the SteadyState scheme is employed, emphasizing a steady state and omitting time derivative terms. The gradient discretization scheme is Gauss Linear. Three distinct convection terms are handled with the bounded Gauss Linear Upwind Grad (U), bounded Gauss Linear Upwind Grad (nuTilda), and Gauss Linear schemes for divergence discretization. The Laplace discretization scheme is specified as Gauss Linear Limited Corrected to 0.33. Surface normal gradient calculations are conducted using the Limited Corrected 0.33 scheme. Linear interpolation is adopted as the interpolation method. In accordance with established empirical practices, the selection of a convergence residual value of 1e−6 is deemed appropriate for addressing the subsonic aerodynamic problem explored in this study. Furthermore, a maximum iteration count of 1 000 is chosen.

2.3 Study on mesh convergence

In general practice, augmenting the number of grid cells results in enhanced computational precision. However, as the grid count increases, so does the computational time and the consumption of computational resources. As data exchange during optimization necessitates in-memory operations, optimization tasks are associated with substantial memory usage. Moreover, the grid count is limited by the available memory, and in practical optimization work, approximately 2 GB of memory is required for approximately 10 000 grid cells. Therefore, to ascertain the requisite grid count for optimization design, a convergence analysis of the flow field grid is imperative.

The O-shaped far field grid adopted in this paper is shown in Fig.3. To balance computational precision and efficiency, it is essential to identify an appropriate grid count. In this study, six sets of flow field grids, all meeting quality criteria, are generated based on different surface grid densities at the leading and trailing edges, as well as varying grid boundary growth rates. These grids are employed to solve the flow field under cruising conditions, and the resulting grid counts and aerodynamic force calculations are summarized in Table 1, where C_L is the lift coefficient.

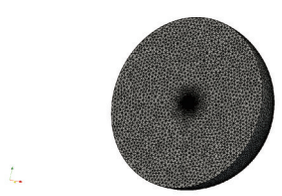

Fig.3 O-shaped far field grid

Table 1 Convergence of mesh with different densities

Grid number/10^4	C_L	C_D	C_L/C_D	Time required for 1 000 steps (64 CPU)/s
38.6	0.130 70	0.019 08	6.849 4	19
75.9	0.130 63	0.016 46	7.937 1	34
104.7	0.129 86	0.016 22	8.008 6	52
134.0	0.129 69	0.016 09	8.060 7	68
185.6	0.129 59	0.016 01	8.094 3	86
213.2	0.129 46	0.015 96	8.111 5	102

As per the analysis conducted above, when the mesh count reaches 104.7 million, the variations in the calculated lift-to-drag ratio are negligible, providing an accurate representation of the aerodynamic shape. Simultaneously, considering factors such as memory consumption, computational efficiency, and precision, it is determined that a mesh of 104.7 million will be utilized for the optimization design.

2.4 Optimization problem description

Preceding the initiation of aircraft aerodynamic shape optimization, it is crucial to formulate a customized mathematical model in accordance with the specific design prerequisites. Consequently, the mathematical model for optimizing the aerodynamic shape of an aircraft is outlined as follows

$$\begin{cases} \min f(x) \quad x \in \mathbf{R}^N \\ \text{s.t. } g_i(x) \leqslant 0;\ i = 1, 2, \cdots, N \\ \quad x_i^l \leqslant x_i \leqslant x_i^u \end{cases} \tag{12}$$

Design variables, objective functions, and constraint functions constitute the triad of essential elements in optimal design. Within the aforementioned equation, x embodies the design variables, specifically, the position vector of 192 FFD control points. The objective function, denoted as $f(x)$, pertains to the drag coefficient C_D. Concurrently, the constraint functions, articulated as $g_i(x)$, encapsulate the ensuing criteria: Angle of attack $\alpha = 1°$, lift coefficient $C_L \geqslant C_{L0}$, volume $V \geqslant V_0$, thickness $0.9T_0 \leqslant T \leqslant 1.5T_0$.

3 Optimization Results

The aircraft's baseline experiences modifications contingent upon the FFD control point's positioning. The distribution of FFD control points is spread across eight cross-sections, each profile has 24 FFD points, with each profile's control points constrained to move horizontally and vertically within the plane, without any displacement in the z-direction. As shown in Fig.4, it is evident that optimization has led to significant changes in the positions of FFD control points at the leading and trailing edges. The movement of control points at the inner-wing and outer-wing junctions is more pronounced compared to those at the fuselage root.

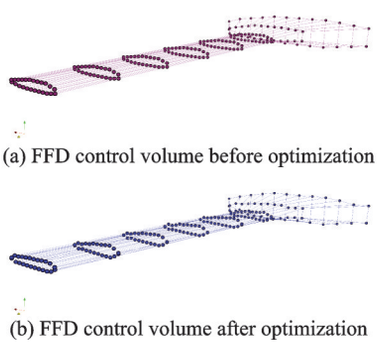

Fig.4 Change of the FFD control volume before and after optimization

The iterative nature of the objective function throughout the optimization process is visually demonstrated in Fig.5. After 31 iterations, achieving a convergence residual of 1e−6, the drag coefficient experiences a reduction from 0.016 2 to 0.015 1. Due to the continued fluctuation of the lift coefficient within a certain range throughout the optimization process, the variation in lift-to-drag ratio more intuitively reflects the enhancement in aerodynamic

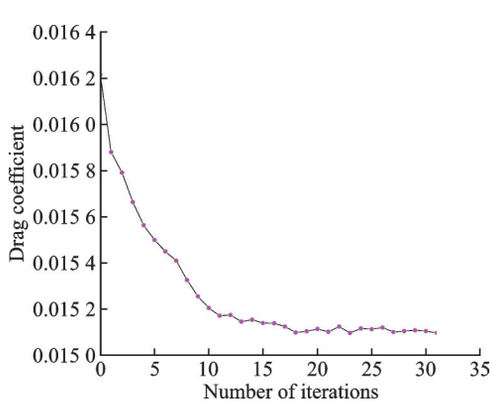

Fig.5 Iteration process of the objective function

performance before and after optimization. Therefore, in Fig.6, a comparison of the lift-to-drag ratios at different angles of attack before and after optimization is presented. It can be observed that under the design condition's angle of attack, there is a significant increase in the lift-to-drag ratio, with an improvement of approximately 7.17%.

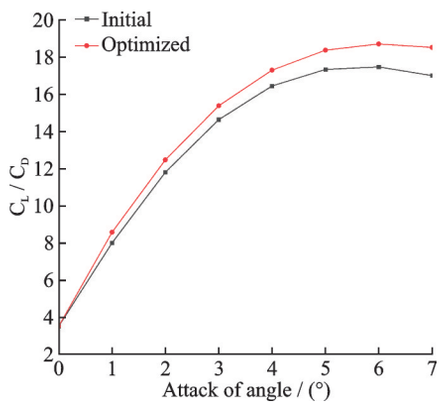

Fig.6 Lift-drag ratio at different angles of attack before and after optimization

Fig.7 vividly illustrates the shifts in pressure distribution across the entire aircraft after the completion of the optimization process. It is evident that optimization results in a pronounced rearward shift of the high-pressure area. During the optimization process, the FFD method brings about modifications in the thickness of each airfoil of the control sections by altering the spatial location vectors of control points. To delve into the specific airfoil alterations pre- and post-optimization for each cross-section, four profiles are selected at distinct locations: near the fuselage root (5.2%), at the fuselage-inner wing junction (10.5%), at the inner wing-outer wing junction (29.6%), and at the wingtip (97.4%), and each of the four cross-section is labeled with the names *A*, *B*, *C*, and *D*, as shown in Fig.7. The airfoil changes and pressure coefficient C_p variations for these four profiles are displayed in Fig.8. The green dashed lines represent the initial shapes, while the purple solid lines represent the optimized shapes. It is apparent from the pressure coefficient distributions before and after optimization that the pressure coefficient curves become smoother.

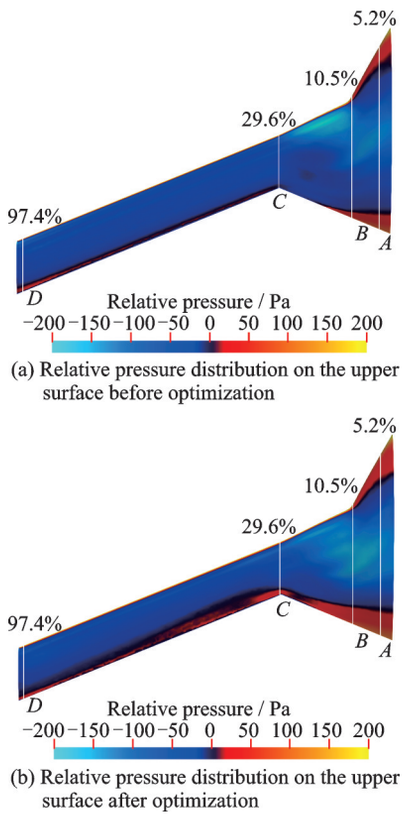

Fig.7 Relative pressure distribution on the upper surface before and after optimization

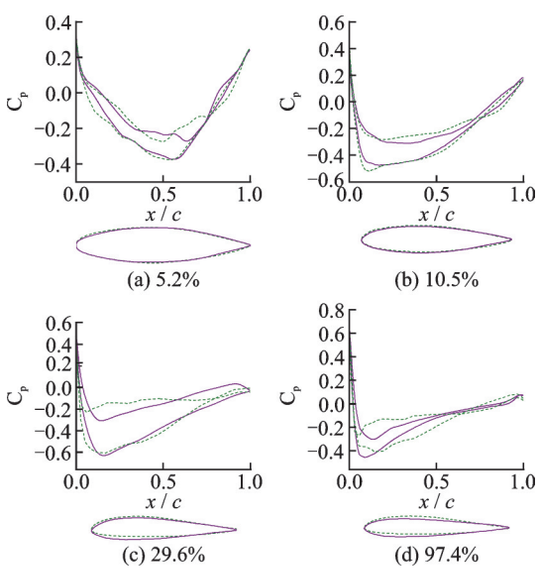

Fig.8 Airfoil profile and pressure coefficient variation of four control profiles

4 Conclusions

(1) Utilizing the free-form deformation method to describe shape parameters, we create a coherent linkage between a sensible number of FFD control

points and the mesh nodes situated on the aerodynamic surface through displacement mapping. By combining this approach with a gradient algorithm grounded in discrete adjoint methods, we realize an effective aerodynamic optimization design method that is well-suited for intricate shapes during the conceptual design phase.

(2) The research focuses on aerodynamic optimization design for a subsonic flying-wing UAV. The optimization process significantly enhances the aerodynamic performance of the flying-wing UAV, resulting in a notable 7.17% increase in the lift-to-drag ratio.

(3) The high-efficiency aerodynamic shape optimization design method established in this study enables rapid iteration of shape design proposals during the conceptual design phase. This significantly boosts the efficiency of aircraft conceptual design and demonstrates its excellent applicability to the layout design of other aircraft with intricate shapes.

References

[1] FENG Z P, LI J, REN B, et al. Evolution calculation in aerodynamic optimization design[J]. Shanghai Steam Turbine, 2003(1): 6-16. (in Chinese)

[2] HICKS R M, HENNE P A. Wing design by numerical optimization[J]. Journal of Aircraft, 1978, 15(7): 407-412.

[3] LEUNG T M, ZINGG D W. Aerodynamic shape optimization of wings using a parallel Newton-Krylov approach [J]. AIAA Journal, 2012, 50(3): 540-550.

[4] NEMEC M, ZINGG D W, PULLIAM T H. Multipoint and multi-objective aerodynamic shape optimization[J]. AIAA Journal, 2004, 42(6): 1057-1065.

[5] CHANG M, SUN Y, BAI J Q, et al. Aerodynamic optimization design of secondary folding wing for tubular UAV with flat angle rotating mechanism constraint[J]. Acta Aeronautica et Astronautica Sinica, 2022, 43(11): 463-474. (in Chinese)

[6] KENWAY G, KENNEDY G, MARTINS J R R A. A CAD-free approach to high-fidelity aerostructural optimization[C]//Proceedings of the 13th AIAA/ISSMO Multidisciplinary Analysis Optimization Conference, Texas: AIAA, 2010.

[7] SEDERBERG T W, PARRY S R. Free-form deformation of solid geometric models[J]. Computer Graphics, 1986, 20(4): 150-161.

[8] HE P, MADER C A, MARTINS J R R A, et al. DAFoam: An open-source adjoint framework for multidisciplinary design optimization with open FOAM [J]. AIAA Journal, 2020, 58(3): 1304-1319.

[9] HE P, MADER C A, MARTINS J R R A, et al. An aerodynamic design optimization framework using a discrete adjoint approach with OpenFoam[J]. Computer & Fluids, 2018, 168: 285-303.

[10] JAMESON A. Aerodynamic design via control theory [J]. Journal of Scientific Computing, 1988, 3(3): 233-260.

[11] ZHANG W W, WU X J, SONG S F. Research on uncertainty and high dimensional problems in aerodynamic shape optimization design[M]. Xi'an: Northwestern Polytechnical University Press, 2020: 48-49. (in Chinese)

Acknowledgement This work was supported in part by the National Natural Science Foundation of China (No. 11972180).

Authors Mr. **AN Yingtao** received the M.S. degree in mechanics from Nanjing University of Aeronautics and Astronautics, Nanjing, China, in 2023. His current research interests include optimization and evaluation of aircraft shape design based on CFD, structural dynamics and aeroelastic analysis.

Prof. **ZHAO Yonghui** received the Ph.D. degree in General Mechanics and Mechanical Fundamentals from Harbin Institute of Technology, Harbin, China, in 1999. He has been affiliated with the College of Aerospace Engineering, Nanjing University of Aeronautics and Astronautics after completing his postdoctoral research at Nanjing University of Aeronautics and Astronautics in 2004, currently serving as a professor and doctoral supervisor. His research primarily encompasses aircraft aeroelasticity, mechanics and control, as well as vibration mechanics and control.

Author contributions Mr. **AN Yingtao** designed the study, complied the models, conducted the analysis, interpreted the results and wrote the manuscript. Dr. **MU Xusheng** contributed to the construction of optimization platform and mesh generation. Prof. **ZHAO Yonghui** contributed to the discussion and background of the study.

All authors commented on the manuscript draft and approved the submission.

Competing interests The authors declare no competing interests.

(Production Editor: ZHANG Huangqun)

基于CFD的飞翼布局无人机气动外形优化

安英韬，沐旭升，赵永辉

(南京航空航天大学航空学院,南京 210016, 中国)

摘要: 飞翼布局因其独特的翼身融合的气动外形,大大提高了飞行器的有效升力面积,外形优化问题和布局优化对于此类构型气动性能的提升同样重要。本文为解决飞翼布局无人机气动外形优化问题,建立了高效的参数化建模方法,实现了适应复杂外形的几何参数化变形控制,将基于梯度的优化算法、离散伴随方法与基于RANS (Reynolds average Navier-Stokes)方程的计算流体力学(Computational fluid dynamics, CFD)方法相结合,对飞翼布局无人机完成了气动外形的优化减阻设计,升阻比提升了7.17%。优化结果表明,在满足约束要求的前提下,基于上述技术的气动优化设计方法对翼身融合类构型具有良好的适应性,能有效改善无人机的气动性能。

关键词: 飞翼布局;气动优化;计算流体力学;伴随方法;自由格式变形